ACS APPLIED MATERIALS & INTERFACES

Research Article

Cite This: ACS Appl. Mater. Interfaces 2018, 10, 42967−42978

www.acsami.org

Exploiting Synergetic Effects of Graphene Oxide and a Silver-Based Metal−Organic Framework To Enhance Antifouling and Anti-Biofouling Properties of Thin-Film Nanocomposite Membranes

Mostafa Dadashi Firouzjaei,[†,#] Ahmad Arabi Shamsabadi,[‡,#] Sadegh Aghapour Aktij,[§] S. Fatemeh Seyedpour,[§] Mohammad Sharifian Gh.,[∥] Ahmad Rahimpour,[*,§] Milad Rabbani Esfahani,[*,†] Mathias Ulbricht,[⊥] and Masoud Soroush[*,‡]

[†]Department of Chemical and Biological Engineering, The University of Alabama, Tuscaloosa, Alabama 35487, United States

[‡]Department of Chemical and Biological Engineering, Drexel University, Philadelphia, Pennsylvania 19104, United States

[§]Department of Chemical Engineering, Babol Noushirvani University of Technology, Shariati Avenue, Babol Mazandaran 4714871167, Iran

[∥]Department of Chemistry, Temple University, Philadelphia, Pennsylvania 19122, United States

[⊥]Lehrstuhl für Technische Chemie II, Universität Duisburg-Essen, D-45117 Essen, Germany

Supporting Information

ABSTRACT: Thin-film composite (TFC) membranes still suffer from fouling and biofouling. In this work, by incorporating a graphene oxide (GO)−silver-based metal−organic framework (Ag-MOF) into the TFC selective layer, we synthesized a thin-film nanocomposite (TFN) membrane that has notably improved anti-biofouling and antifouling properties. The TFN membrane has a more negative surface charge, higher hydrophilicity, and higher water permeability compared with the TFC membrane. Fluorescence imaging revealed that the GO−Ag-MOF TFN membrane kills *Escherichia (E.) coli* more than the Ag-MOF TFN, GO TFN, and pristine TFC membranes by 16, 30, and 92%, respectively. Forward osmosis experiments with *E. coli* and sodium alginate suspensions showed that the GO−Ag-MOF TFN membrane by far has the lowest water flux reduction among the four membranes, proving the exceptional anti-biofouling and antifouling properties of the GO−Ag-MOF TFN membrane.

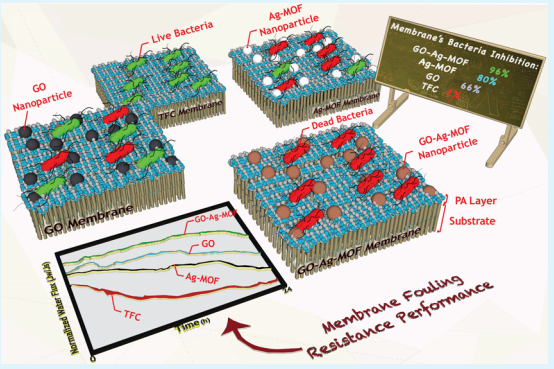

KEYWORDS: *anti-biofouling, antifouling, metal−organic framework, graphene oxide, thin-film nanocomposite membrane*

1. INTRODUCTION

The demand for fresh water is increasing, and the limited nature of fresh water resources has motivated the development of novel technologies for water purification.[1,2] The membrane technology can greatly contribute to water and wastewater treatment due to its compactness, simplicity, and sustainability.[3,4] Among membrane-based processes, forward osmosis (FO) is attractive for its high energy saving and hydraulic pressure independency.[5−8]

Thin-film composite (TFC) membranes have applications in industrial desalination and wastewater treatment.[9] However, their fouling and biofouling in water streams containing dissolved organic matters and microorganisms negatively impact their stability and durability. Microorganism adhesion to the surface of TFC membranes results in the distribution and proliferation of microorganisms, leading to the formation of extracellular polymeric substances on TFC surfaces, which reduces water flux, enhances required energy, and shortens membrane lifetime. Therefore, developing membranes with anti-biofouling and antifouling properties is of great significance.[10−13]

The biocidal agents have been used to prevent attachment of the living cells to the outer surface of the membranes.[5] Nanoparticles (NPs) from metal- or metal oxide-containing compounds such as silver-based materials,[14] titanium dioxide,[15,16] zinc oxide,[17] carbon-based compounds, and copper[18] can be employed to tailor the properties of the membranes and improve their antifouling and anti-biofouling activities.[19−22] Among these NPs, silver NPs have outstanding antibacterial properties against bacteria, viruses, and fungi.[23] However, their incorporation into the selective layers of TFC membranes is still challenging because (i) NPs are easily washed out, leading to loss of their antibacterial activity against microorganism and (ii) low compatibility of NPs with polymer networks results in

Received: July 27, 2018
Accepted: November 9, 2018
Published: November 9, 2018

DOI: 10.1021/acsami.8b12714
ACS Appl. Mater. Interfaces 2018, 10, 42967−42978

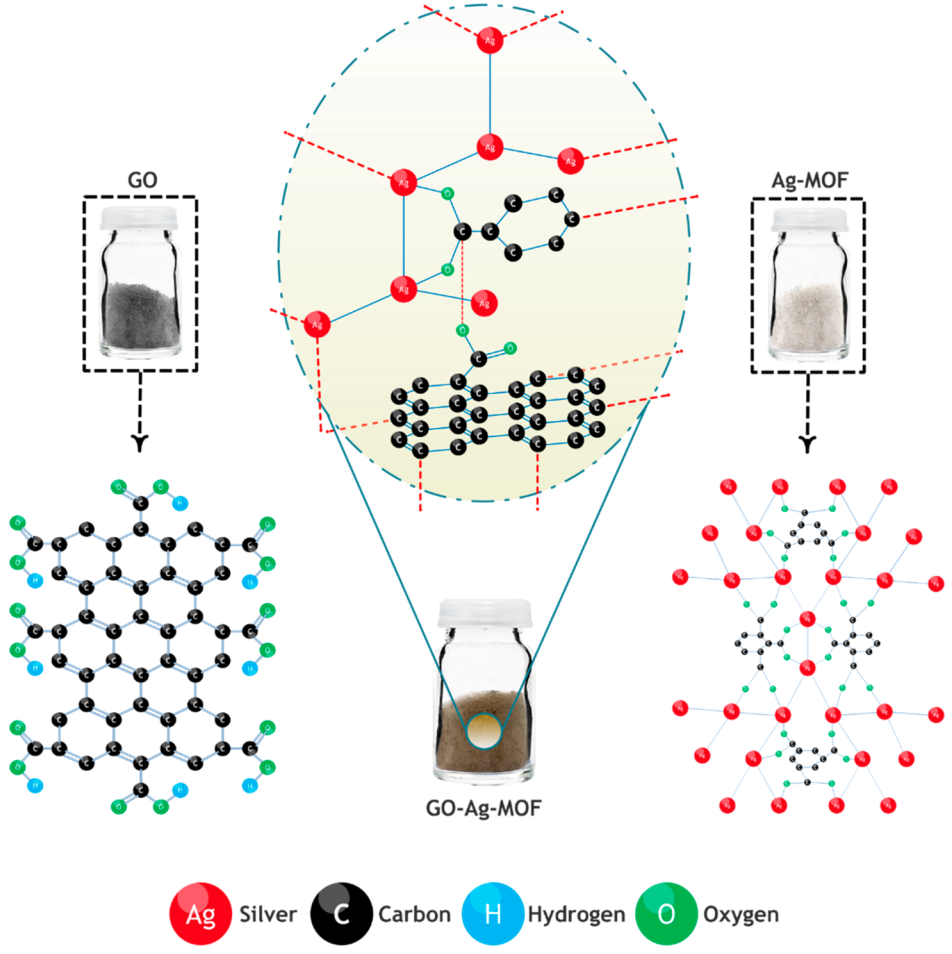

Figure 1. Chemical formulas of the nanomaterials (GO, Ag-MOF, and GO−Ag-MOF).

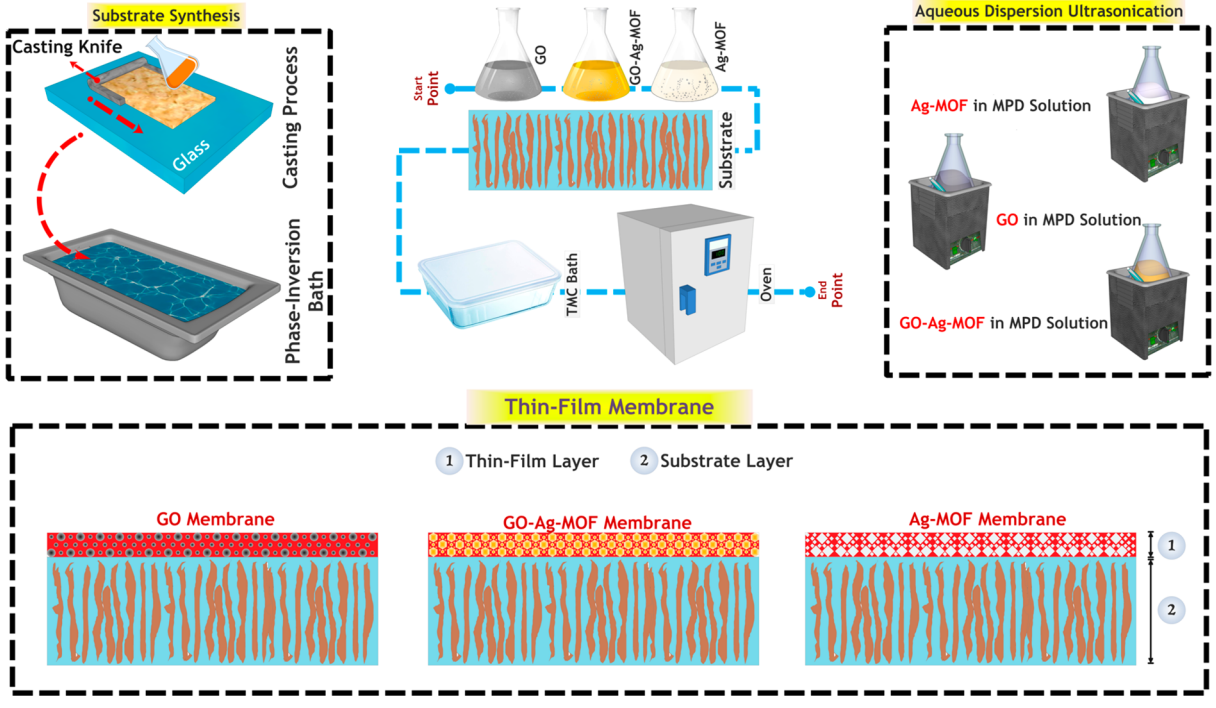

Figure 2. Steps in the fabrication of the TFN membranes.

DOI: 10.1021/acsami.8b12714
ACS Appl. Mater. Interfaces 2018, 10, 42967−42978

defect formation and deterioration of thin-film nanocomposite (TFN) membrane performance.

Metal−organic frameworks (MOFs) are networks consisting of metals and organic linkers.[24] Silver-based MOFs have demonstrated potent biocidal properties due to their silver clusters surrounded by organic ligands.[25] The main antibacterial mechanism of the MOFs is the long-lasting metal ion release, which leads into bacteria cell damage and death.[25−27] Porous structures of MOFs allow for long-lasting interactions between bacteria cells and metal ions, and organic ligands of MOFs control ion release. The structure of MOFs also prevents the metal ions from reacting with other agents and having unwanted interactions.[28−30] Furthermore, organic parts of MOFs provide functional groups for modification.

Graphene oxide (GO) also has remarkable antibacterial properties.[31] GO's antibacterial properties come from chemical and physical interactions between bacteria cells and GO nanosheets.[32,33] Sharp edges of GO nanosheets, oxidative stress, and superoxide anions generated by GO are responsible for the GO's biocidal activity.[34,35] Our previous study showed that decorating an Ag-MOF with GO leads to a GO−Ag-MOF nanocomposite that has superior antimicrobial properties.[14] When a nanomaterial is hydrophilic and has a negative charge, incorporating the nanomaterial into a TFC selective layer forms a hydration layer which separates the TFC and the feed solution lowering the fouling rate.[16,36,37]

In this work, for the first time, we embedded hydrophilic GO−Ag-MOF nanomaterials with high negative surface charges into the polyamide (PA) selective layer. We then fabricated and characterized GO−Ag-MOF, Ag-MOF, and GO TFN FO membranes. We studied the transport properties of the TFN membranes as well as the pristine TFC membrane. Furthermore, the antifouling and anti-biofouling activities of the fabricated membranes were evaluated in FO experiments using sodium alginate and *E. coli* suspensions, respectively.

2. MATERIALS AND METHODS

2.1. Materials and Chemicals. Ultrason E6020P polyethersulfone (PES) with molecular weight (M_w) of 58 000 g/mol was purchased from BASF, Germany. GO was supplied by US Research Nanomaterial. *N*,*N*-dimethylformamide (DMF) with purity of >99.5%, polyvinyl pyrrolidone (PVP) with M_w of 25 000 g/mol, 1,3-phenylendiamine (MPD, >98%), trimesoylchloride (TMC, >98%), *n*-hexane (>95%), sodium chloride (NaCl, >99.5%), 1,3,5-benzentricarboxylic acid (>99%), silver nitrate ($AgNO_3$, >99%), and ethanol with purity of >99% were purchased from Merck, Germany. Propidium iodide, sodium dodecyl sulfate (SDS, >99%), and terrific broth were acquired from Sigma-Aldrich. *E. coli* 35695 was supplied by ATCC Co., and SYTO9 was supplied by Molecular Probes.

2.2. Nanomaterials Synthesis and Thin-Film Membranes Fabrication and Characterization. Silver-based nanomaterials (Ag-MOF and GO−Ag-MOF) were synthesized using the ultrasonic irradiation method.[14] The details of nanomaterial synthesis can be found in our previous work.[14] Figures 1 and S1 show chemical formulas of the nanomaterials.

Figure 2 schematically depicts how the TFN membranes were fabricated using interfacial polymerization (IP). The PES substrate was created via the phase separation technique. This involved casting a solution of PES (16 wt %) and PVP (1 wt %) in DMF (83 wt %) followed by immersing the cast into the coagulation bath containing water, DMF (1 wt %), and SDS (0.1 wt %). For the thin-film membrane fabrication, first 0.03 wt % of the nanomaterials was dispersed in a 2 wt % MPD aqueous solution using 30 min ultrasonication. The PES substrate was then submerged in the MPD solution for 2 min. After removing the excess MPD solution using an air-knife, the substrate was then submerged in a 2% TMC in *n*-hexane solution for 25 s. Finally, the fabricated membrane was fast dried (5 min) at 80 °C using an oven. TFN membranes containing GO, Ag-MOF, and GO−Ag-MOF nanomaterials were fabricated. Also, a TFC membrane without any nanomaterials was prepared.

Field emission scanning electron microscopy (FE-SEM) (Zeiss Supra 50VP) and energy-dispersive X-ray (EDX) spectroscopy with an Everhart−Thornley detector and a Schottky field emission electron gun were employed to visualize the structure and elemental compositions of the TFC and TFNs. The topography of the membrane surface was evaluated using atomic force microscopy (AFM) (Bruker Dimension Icon instrument) with Sb-doped silicon probes (tip radius = 10 nm and spring constant = 42 N/m) under a tapping mode with a scanning rate of 0.5 Hz. The scan area was 3 μm × 3 μm. A contact angle measuring device (G10, KRUSS, Germany) equipped with an image processing software was used to assess the hydrophilicity of the membranes. The reported contact angles are mean of five positions on the surface of each membrane. Fourier-transform infrared (FTIR) spectroscopy with a deuterated-triglycine sulfate detector with 64 scans at a resolution of 4 cm^{-1} was used to verify functional groups of the membranes. X-ray photoelectron spectroscopy (XPS) (Physical Electronics VersaProbe 5000 spectrometer) was carried out to verify the embedment of the nanomaterials in the TFN membranes. To calculate the silver-ion release rate of the TFNs, 6.45 cm^2 coupons of the membranes were stored overnight in deionized (DI) water (20 mL) under mild shaking, followed by acidifying the coupons with a 1% nitric acid solution and then shaking the samples at 80 rpm for 30 days. Next, the water samples and the TFN membranes were analyzed (after 1, 7, and 30 days). The concentration of the released silver ions was determined using inductively coupled plasma mass spectroscopy (ICP-MS PerkinElmer NexION 300X).[38] The surface charge of both nascent TFC and TFN membranes was evaluated by Anton Paar SurPASS electrokinetic solid surface zeta potential analyzer (Anton Paar USA, Ashland, VA). The potentials were measured using a 1 mM KCl electrolyte solution in a pH range of 5−10 at 25 °C. Zeta potentials of the films were calculated based on the Helmholtz−Smoluchowski equation. Two separate samples of each membrane were assessed to minimize measurement uncertainties.

2.3. Transport, Antifouling, and Anti-Biofouling Properties. An FO setup shown in Figure S2 (in the Supporting Information) was used to assess the properties of the TFC and TFN membranes. Water permeability (A) and solute permeability (B) coefficients as well as anti-biofouling and antifouling properties of the membranes were determined using the protocol discussed in our previous paper.[5] Sodium alginate (250 mg/L) and *E. coli* bacteria (10^7 cfu/mL) suspensions were used for fouling and biofouling experiments, respectively. For these experiments, the draw and feed solutions had volumes of 3 L. During the 24 h operation, the cross-flow velocity was kept at 8.5 cm/s. Three measurements from two independent experiments were made. The mean of each of the three measurements are reported in this article. Detailed information about biocidal activity assessment and fluorescence imaging (FI) can be found in our previous published paper.[5,14]

3. RESULTS AND DISCUSSION

3.1. Nanomaterial Characterization. The nanomaterials were characterized using techniques described in ref 14. The transmission electron microscopy (TEM) image (Figure 3) confirms the formation of a unique GO−Ag-MOF nanocomposite. Proper dispersity of the Ag-MOF NPs on the GO nanosheets was observed.[14] Average sizes of 160, 33, and 78 nm were obtained from dynamic light scattering for the nanocomposite, MOF, and GO nanomaterials with 0.5 molarity dispersion in the DI water, respectively.[14] The formation of the GO−Ag-MOF nanocomposite was verified by XPS, showing a high concentration of silver and carbon in Ag-MOF and GO−Ag-MOF, respectively. Additionally, other

DOI: 10.1021/acsami.8b12714
ACS Appl. Mater. Interfaces 2018, 10, 42967−42978

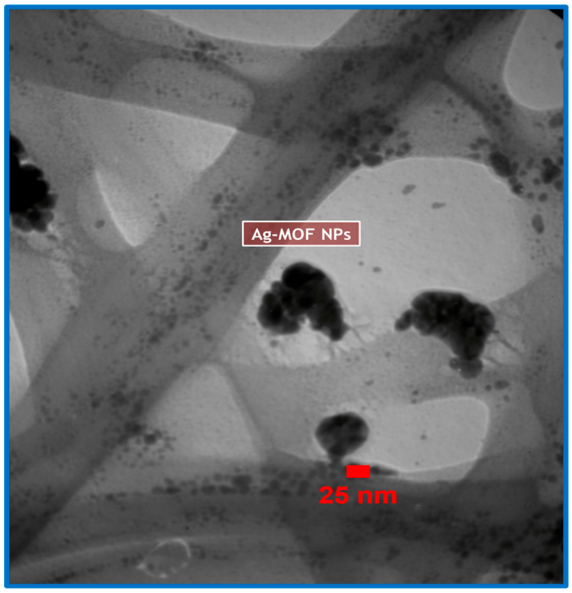

Figure 3. TEM image of the GO−Ag-MOF nanomaterial (25 nm resolution).

analyses of the nanomaterials verify the decoration of the Ag-MOF NPs with GO.[14]

3.2. Membranes Characterization. Surface morphological and structural changes of the TFN membranes were monitored using SEM (Figures 4−6) and AFM techniques

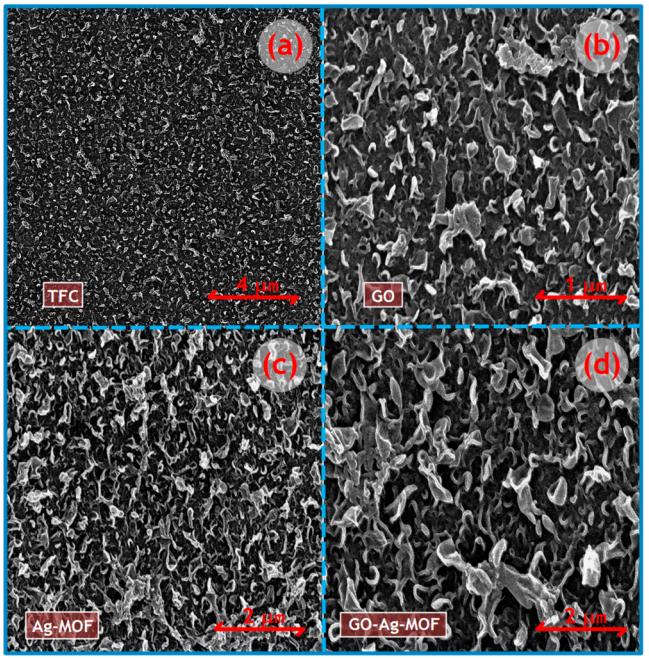

Figure 4. Top surface SEM images of (a) the TFC, (b) GO TFN, (c) Ag-MOF TFN, and (d) GO−Ag-MOF TFN membranes.

(Table 1). A typical ridge-and-valley structure was observed for the TFC membrane. The applied modifications on the membrane increased the membrane surface roughness, pointing to the embedment of the nanomaterials in the top surface. The enhanced surface roughness together with the cross-sectional images of the membrane confirmed the creation of the sub-500 nm thin-film layer. In Figure 5d, the red line

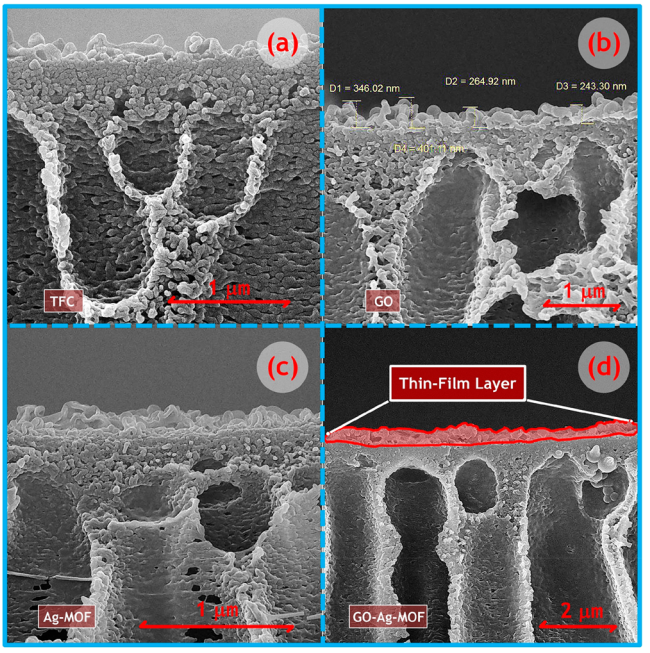

Figure 5. Cross section SEM images of (a) the TFC, (b) GO TFN, (c) Ag-MOF TFN, and (d) GO−Ag-MOF TFN membranes.

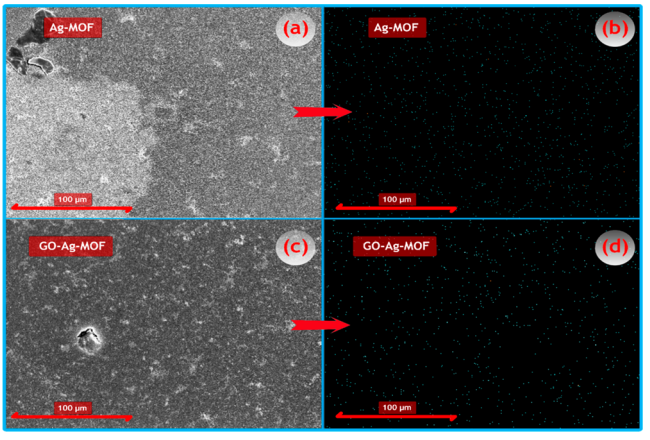

Figure 6. (a) Top surface image of the Ag-MOF membrane, (b) silver-ion EDX mapping of the Ag-MOF membrane, (c) top surface image of the GO−Ag-MOF membrane, and (d) silver-ion EDX mapping of the GO−Ag-MOF membrane.

Table 1. Surface Roughness and Contact Angles of the Membranes

membrane	surface roughness (nm) S_a[a]	S_q[a]	contact angle (deg)
TFC	87 ± 12	108 ± 14	71 ± 4
GO	133 ± 8	166.±17	57 ± 2
Ag-MOF	386 ± 6	442 ± 19	62 ± 3
GO−Ag-MOF	232 ± 13	273 ± 9	54 ± 3

[a] S_a: mean roughness. S_q: RMS roughness.

around the thin-film layer of the GO−Ag-MOF TFN membrane reveals the formation of the thin-film layer. In addition, EDX of the TFN membranes (Figure 6, Table S1 and Figures S3 and S4 in the Supporting Information) detected the silver element in the PA layer of the MOF containing membranes.

DOI: 10.1021/acsami.8b12714
ACS Appl. Mater. Interfaces 2018, 10, 42967−42978

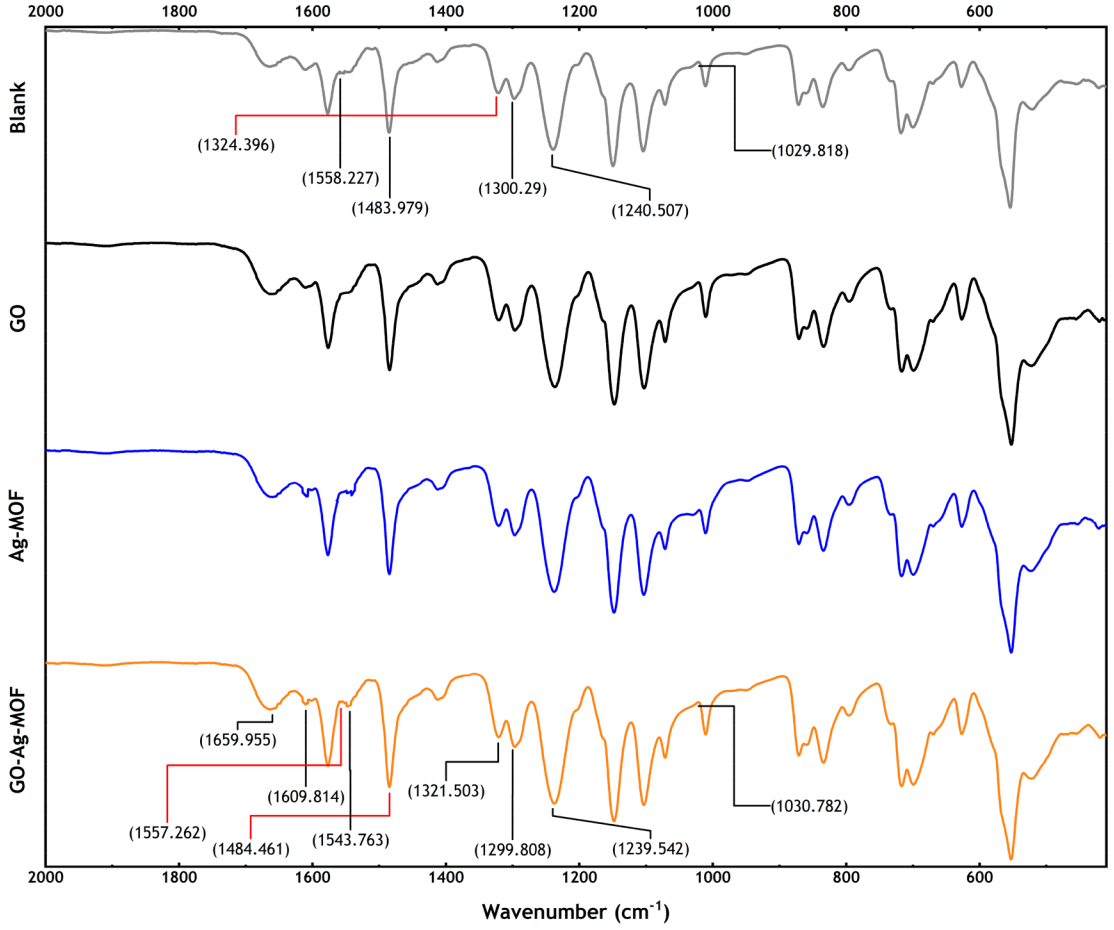

Figure 7. ATR−FTIR spectra of the TFC and TFN membranes.

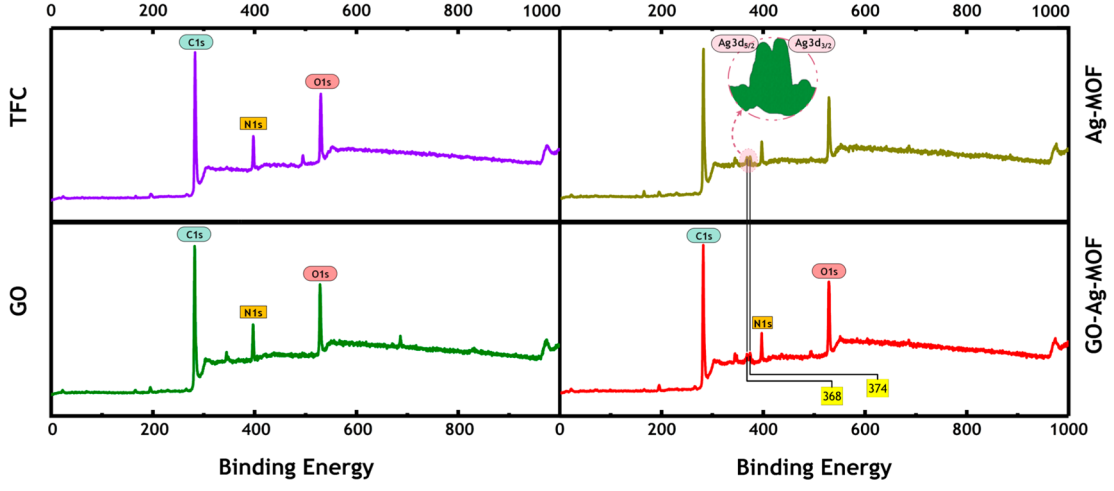

Figure 8. XPS spectra of the fabricated membranes. Note that the other unlabeled peaks represent the material used for the sample preparation (e.g., the peak around 680 eV represents the fluorine used in the XPS instrument vacuum process).

The surface roughness of each fabricated membrane was determined using AFM images. Contact angles are listed in Table 1. The order of the surface roughness values is Ag-MOF TFN > GO−Ag-MOF TFN > GO TFN > TFC. The presence of the NPs, external additives, inside the PA layer changes the morphology of the membrane surface in a way that leads to higher surface roughness. The surface roughness increase depends on the size and the number of the NPs in the PA layer. Incorporating nanomaterials improves the hydrophilicity of the TFN membrane. Synergistic effects of GO and the Ag-MOF, which is due to different hydrophilic functional groups in the structure of the GO−Ag-MOF nanomaterials, endow the TFN membrane with the highest level of hydrophilicity (the lowest contact angle).

The surface chemistry of each membrane was characterized using attenuated total reflection (ATR)−FTIR spectroscopy to verify the successful embedment of the nanomaterials into the TFN membranes (Figure 7). The peak related to the vibration

DOI: 10.1021/acsami.8b12714
ACS Appl. Mater. Interfaces 2018, 10, 42967−42978

Table 2. Elemental Compositions and Significant Peak Characteristics of the Membranes Derived From the XPS Spectra

	C (1s)			O (1s)			Ag (3d)				
membrane	species	energy (eV)	AC[a]%	species	energy (eV)	AC %	species	energy (eV)	AC %	N 1s	O/N ratio
TFC	C−C/C−H	285.0	81.11	N−C═O*/O−C═O*	531.8	9.29				9.60	1.03
	C−N	286.5		*O−C═O	533.3						
	O═C−O/O−C═O	288.0									
GO	C−C/C−H	285.0	75.00	N−C═O*/O−C═O*	531.8	14.50				10.50	1.38
	C−N	286.5		*O−C═O	533.3						
	O═C−O/O−C═O	288.0									
Ag-MOF	C−C/C−H	285.0	86.65	N−C═O*/O−C═O*	531.8	8.72	Ag $3d_{5/2}$	368	0.10	4.53	1.92
	C−N	286.5		*O−C═O	533.3		Ag $3d_{3/2}$	374			
	O═C−O/O−C═O	288.0									
GO−Ag-MOF	C−C/C−H	285.0	81.99	N−C═O*/O−C═O*	531.8	10.50	Ag $3d_{5/2}$	368	0.02	7.49	1.40
	C−N	286.5		*O−C═O	533.3		Ag $3d_{3/2}$	374			
	O═C−O/O−C═O	288.0									

[a]AC: atomic concentration.

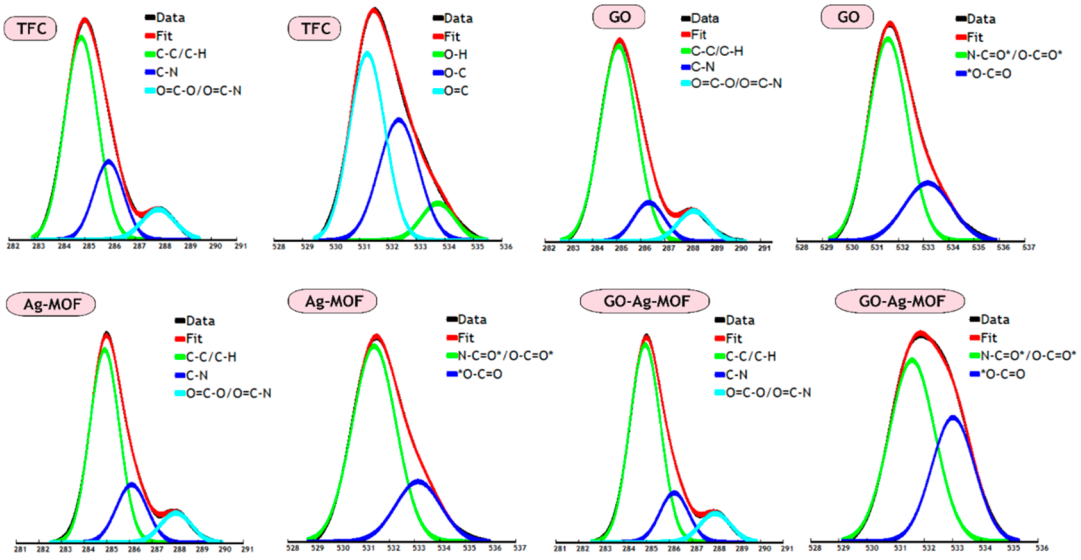

Figure 9. Deconvoluted high-resolution XPS spectra (C 1s and O 1s) for the TFC, GO, Ag-MOF, and GO−Ag-MOF membranes.

of C−C groups in the aromatic rings appeared at 1484 cm^{-1},[39,40] the peaks corresponding to the stretching vibrations of O═S═O can be found at 1300 and 1320 cm^{-1}, and the vibration ascribed to the asymmetric C−O−C group of the PES support layer was detected at 1240 cm^{-1}.[41] The characteristic peaks observed at 1660 cm^{-1} (C═O of amide I), 1544 cm^{-1} (N−H and C−N of the amide II, −CONH−), and at 1610 cm^{-1} (N−H of amide) are related to the PA layer.[42] The intensity reduction at 1610 cm^{-1} for the Ag-MOF and GO−Ag-MOF TFN membranes is most likely related to the interfacial interactions (hydrogen bonds) of the corresponding nanomaterials and the selective layer chains.[43] Likewise, compared with the TFC membrane, a higher level of the carboxyl group (C═O bond) in the TFN membranes caused an intensity enhancement at around 1558 and 1483 cm^{-1}. The considerable bond intensity decrease at 1544 cm^{-1} points to possible interactions between nanomaterials and the PA network because it was not detected in the TFC membrane spectrum. Finally, the bond deformation at 1030 cm^{-1} for GO and GO−Ag-MOF TFN membranes can be ascribed to the epoxy groups of the GO and GO−Ag-MOF nanomaterials.[44,45]

The chemical bonds and elemental compositions of the membranes were obtained via conducting XPS. Figure 8 depicts the XPS survey spectra of the membranes; it shows three peaks at 532, 399, and 285 eV, which are related to the predominant elements including oxygen (O 1s), nitrogen (N 1s), and carbon (C 1s), respectively.[46] In addition, at 368 and 374 eV, two relatively small peaks corresponding to Ag $3d_{5/2}$ and Ag $3d_{3/2}$ appeared in the spectra of the MOF-containing TFN membranes.[46−48] Estimated Ag contents are in acceptable agreement with the results of the complementary analyses using EDX (cf. Table 1).

The elemental compositions of the films are listed in Table 2 indicating the existence of the silver in TFN-containing silver-based nanomaterials. Figure 9 shows the deconvoluted C 1s and O 1s high-resolution XPS spectra. For the C 1s case, three peaks were obtained including: (i) the peak at 285 eV corresponding to C−C or C−H bonds,[49−51] (ii) the peak at 286.5 eV ascribed to C−N bond, and (iii) the peak at 288 eV attributed to O═C−O and O═C−N bonds.[52] Furthermore, for the O 1s case, two peaks at 531.8 and 533.3 eV can be ascribed to the N−C═O*/O−C═O* and *O−C═O bonds, respectively.[53,54]

DOI: 10.1021/acsami.8b12714
ACS Appl. Mater. Interfaces 2018, 10, 42967−42978

The O/N ratio range is between 1.0 and 2.0 (1.0 denotes a fully cross-linked structure with a dense PA layer and high selectivity, and 2.0 represents a fully linear structure with numerous free carboxylic acid functional groups with enhanced hydrophilicity and permeability). The O/N ratio enhancement gained by incorporating the nanomaterials cannot be a representative of a less cross-linked PA. Indeed, all of the nanomaterials comprise functional groups containing oxygen (carboxyl in all nanomaterials, and hydroxyl, and epoxy in GO containing nanomaterials), and this mainly alters the cross-linking ratio of the membranes bearing nanomaterials. High-resolution XPS spectra of C 1s and O 1s provide more information on chemical bonding of all membranes (Figure 9). The considerable increase of the *O−C═O bond in the TFN membrane incorporated by the GO−Ag-MOF nanocomposite is related to the nanocomposite, providing numerous terminated groups (oxygen containing groups in GO and carboxyl terminals in Ag-MOFs).

Figure 10 shows the surface charges of the films at different pHs. The negative surface charge of the TFC membrane is

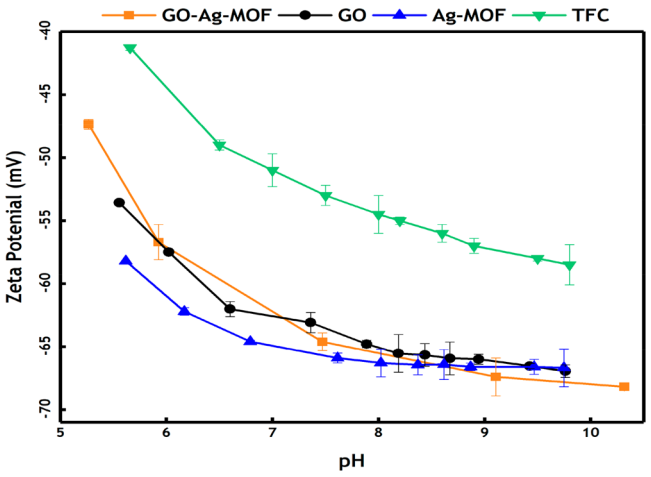

Figure 10. Zeta potential of the fabricated membranes at different pH values.

related to the protonation and deprotonation of the different groups in the PA structure. The protonation of the free amines at low pHs led to a negative surface charge. The deprotonation of the carboxylic acid groups at higher pHs provided more negatively charged surface for the membrane. Incorporating the nanomaterials into the PA layer provides the TFN membranes with a more negative surface charge than the TFC membrane. This alteration is ascribed to the functional groups bearing oxygens of the nanomaterials that are deprotonated at high pH values rendering more negative charges. The Ag-MOF and GO−Ag-MOF TFN membranes showed the most negative zeta potential compared with the GO TFN and TFC membranes owning to the existence of more free −COOH groups in their networks.

3.3. Anti-Biofouling and Antifouling Properties of Membranes. As it was discussed in our previous work,[14] the GO−Ag-MOF nanomaterials showed superior antimicrobial properties. Antibacterial properties of the membranes were evaluated by statically exposing the membranes to *E. coli* for 3 h (Figure 11). FI indicated that the GO−Ag-MOF TFN membrane has outstanding biocidal activity with 96% bacterial growth inhibition (Figure 11d). The bacteria inhibition of the TFC as well as the GO and Ag-MOF TFN membranes were 2, 66, and 80%, respectively. In our previous study,[14] different techniques showed the higher toxicity of GO−Ag-MOF against the *E. coli* bacteria compared with those of the Ag-MOF and GO membranes. Extirpation rates of 95 and 85% of live bacteria cells were achieved for the GO−Ag-MOF and Ag-MOF membranes, respectively. More potent antibacterial properties of the GO−Ag-MOF than other two nanomaterials provided more biocidal activity to the corresponding TFN. The order of the toxicities of the membranes agrees well with the antimicrobial strength of the nanomaterials in the suspension form.

Fouling and biofouling resistances of the TFN membranes were also assessed through FO experiments with a 24 h filtration time and feeds containing sodium alginate and *E. coli*. At least three different samples of each membrane type were tested (Figure 12). The GO−Ag-MOF TFN membrane showed the highest antifouling resistance, as it showed the lowest water flux decrease of 25 ± 3% after contact with alginate (Figure 12a). However, the GO TFN, Ag-MOF TFN, and TFC membranes showed water flux decreases of 38 ± 2, 54 ± 3, and 70 ± 5%, respectively. The GO−Ag-MOF TFN membrane also showed steady water flux with a feed containing *E. coli*, pointing to the enhanced biofouling resistance of the membrane. However, the water flux of the Ag-MOF and GO TFN, and TFC membranes decreased by 34 ± 3, 54 ± 3, and 72 ± 3%, respectively (Figure 12b).

Figure 13 schematically shows the parameters contributing to the biofouling and fouling resistances of the membranes. Furthermore, the main functional groups of the PA layer of each membrane are presented in Figure 13. High biocidal activity, low surface roughness, high negative surface charge, and high hydrophilicity contribute to the biofouling and fouling resistances of the TFN membranes. The outstanding biofouling resistance of the GO−Ag-MOF TFN membrane in comparison to the Ag-MOF TFN, GO TFN, and pristine TFC membranes is ascribed to the low zeta potential and potent biocidal activity of the GO−Ag-MOF. Because of the negative charge of the bacteria cells in pH values between 4 and 9, and the more negative charge of the GO−Ag-MOF, the Ag-MOF TFN membrane surface repulses the bacteria more strongly, decreasing the interactions between the membrane and the bacteria. Besides its high negative zeta potential, the GO−Ag-MOF TFN membrane has the highest biocidal activity, providing more toxic surface. Besides these factors, the highest hydrophilicity of the GO−Ag-MOF TFN membrane minimizes bacteria attachment to the membrane surface, providing the most stable membrane performance. As discussed earlier, the GO−Ag-MOF membrane demonstrated the highest resistance to fouling compared with other membranes. Low contact angle, low surface roughness, and low zeta potential contribute to this performance. Although the surfaces of the TFN membranes are rougher than the TFC membrane, their more negative surface charge and their higher hydrophilicity provided more fouling resistance for the TFN membranes. The GO TFN membrane has a flatter surface and higher hydrophilicity than the Ag-MOF TFN membrane, resulting in higher fouling resistance. Considering the negatively charged sodium alginate, a more negatively charged membrane might result in a greater repulsion of the foulant from the surface, which supports the better antifouling property of the GO−Ag-MOF membrane than the GO membrane. In both biofouling

DOI: 10.1021/acsami.8b12714
ACS Appl. Mater. Interfaces 2018, 10, 42967−42978

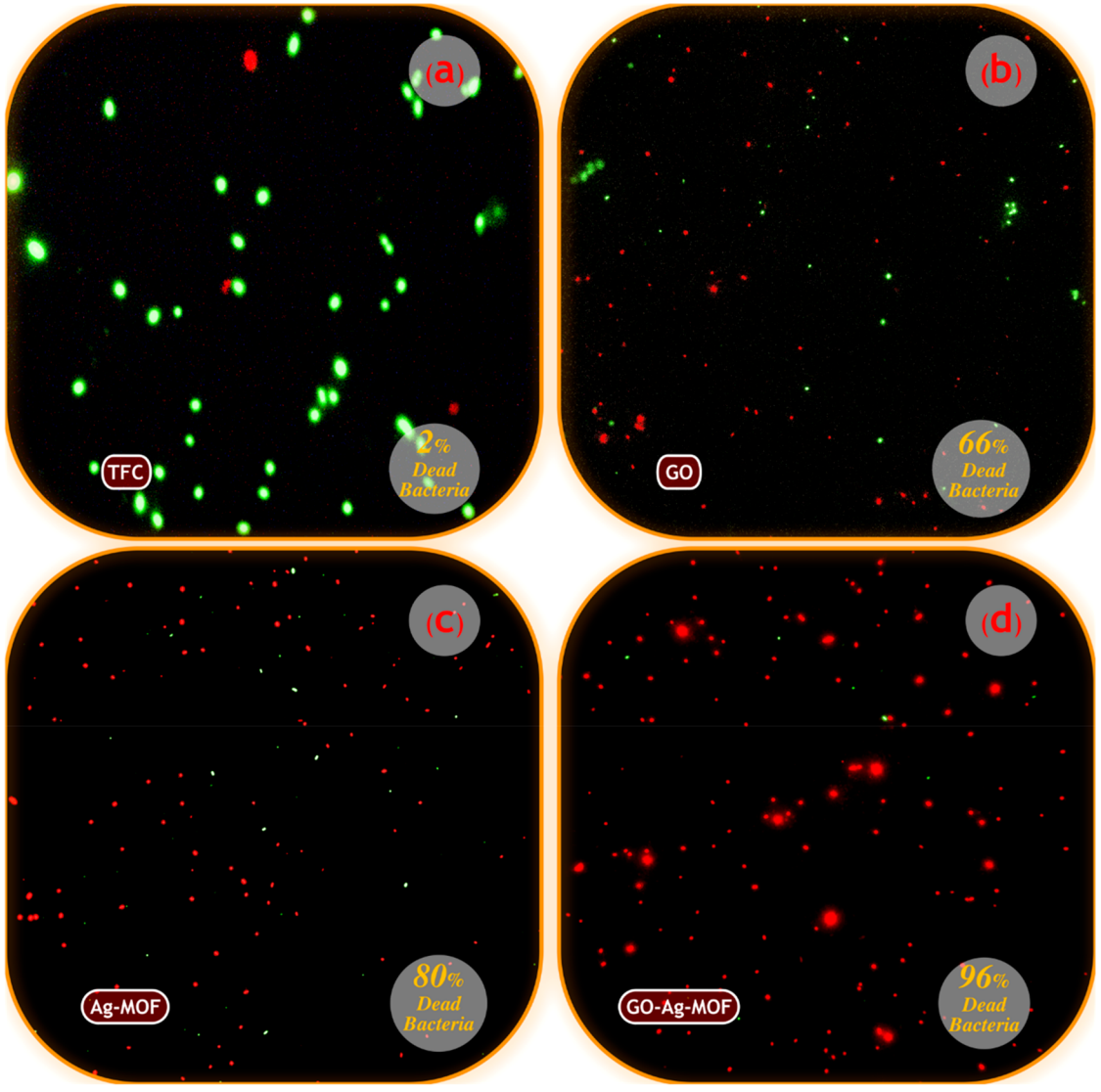

Figure 11. Fluorescence images of the membranes after incubation with *E. coli*: (a) TFC, (b), GO TFN, (c) Ag-MOF TFN, and (d) GO−Ag-MOF TFN.

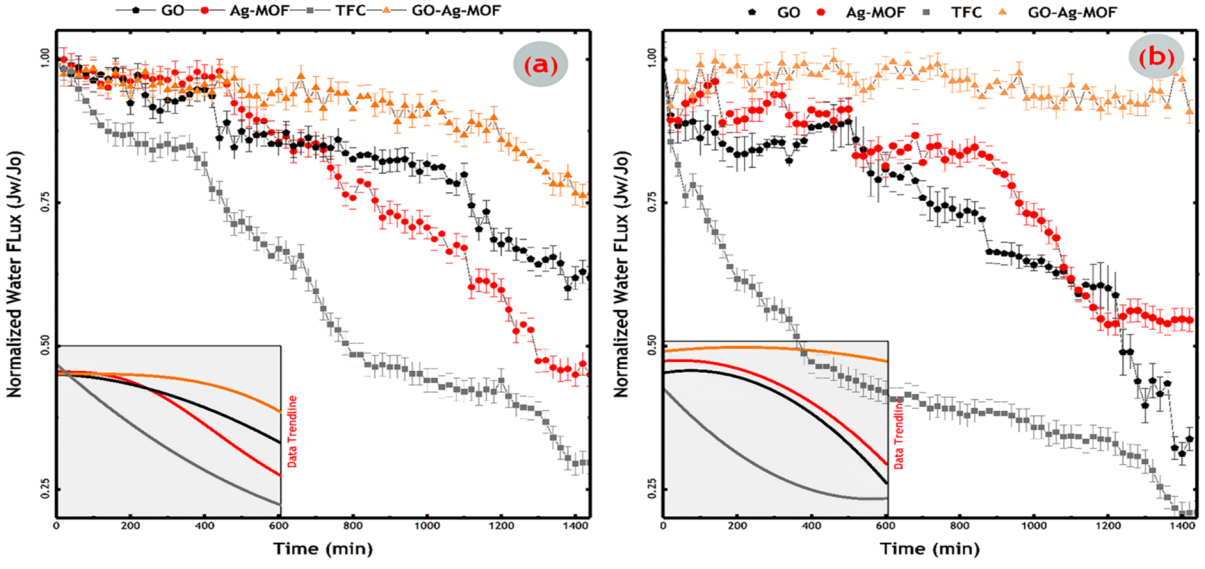

Figure 12. Normalized water fluxes of the membranes: (a) sodium alginate suspension, and (b) *E. coli* suspension.

DOI: 10.1021/acsami.8b12714
ACS Appl. Mater. Interfaces 2018, 10, 42967−42978

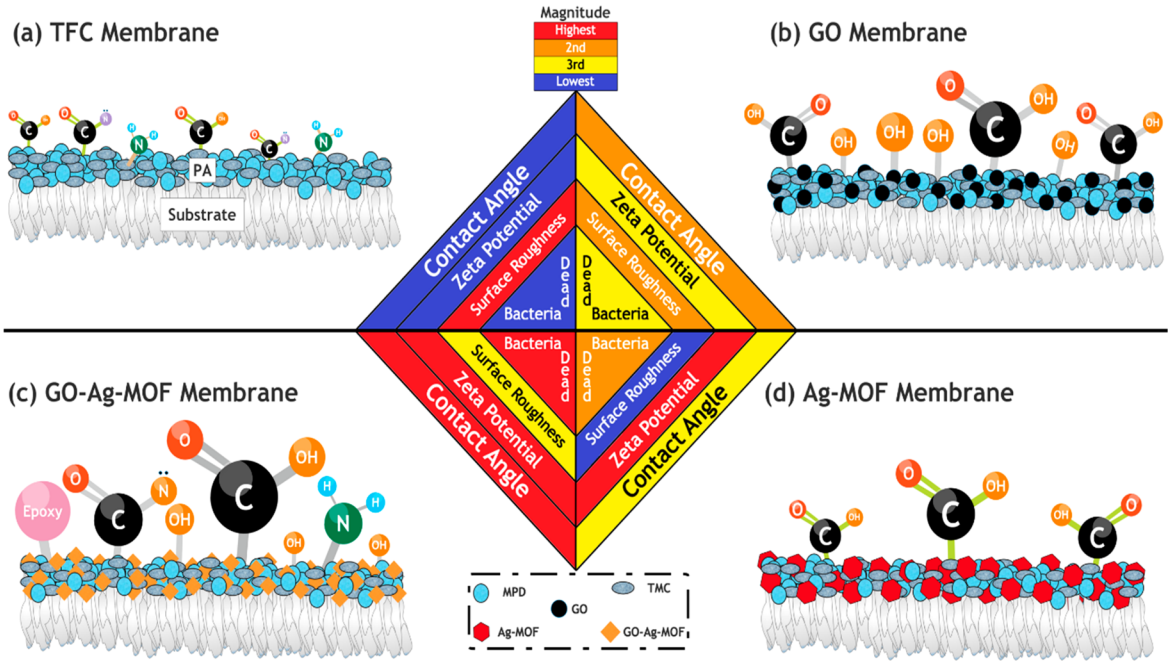

Figure 13. Parameters contributing to anti-biofouling and antifouling properties of the membranes: (a) TFC, (b) GO TFN, (c) GO−Ag-MOF TFN, and (d) Ag-MOF TFN.

and fouling experiments, the TFC membrane had the lowest performance.

3.4. Stability and Silver Ion Release. Since the antibacterial activities of the TFN membranes essentially depend on the continuous release and the concentration of silver ions,[55] the rates of the silver ions released from the Ag-MOF and GO−Ag-MOF TFN membranes were determined using ICP-MS during 30 days. As shown in Figure 14, both of

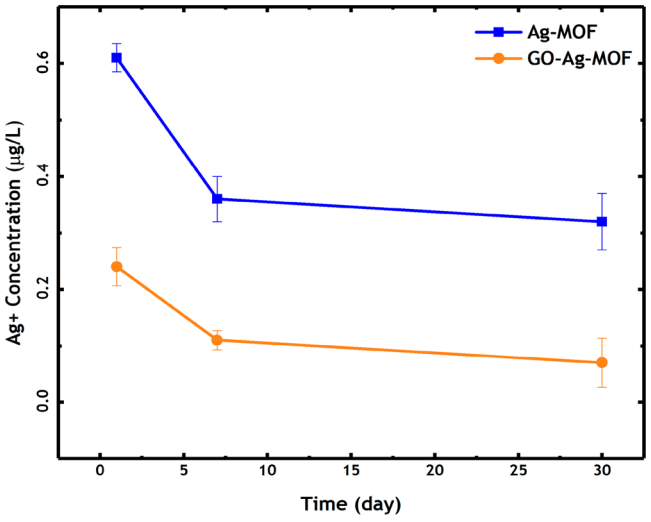

Figure 14. Silver-ion leaching examination of the MOF containing membranes.

the Ag-MOFs and GO−Ag-MOFs TFN membranes display a similar release profile for Ag^+; a sharp release rate at the initial 7 days followed by a gradual depletion to reach a plateau during 30 days. However, both the initial and the final release rates of Ag^+ from the Ag-MOF TFN membrane are considerably greater (nearly 3 times) than those of the GO−Ag-MOF membrane. GO nanosheets in the GO−Ag-MOF nanocomposite serve as mats for Ag-MOF NPs deposition and protect the NPs from rapid Ag^+ release. In other words, Ag-MOF NPs decorate GO and are distributed on its sheets owning to the functional groups bearing oxygen with negative charge that offer reactive sites to adsorb the silver protons existing in the system,[56−59] leading to an effective and prolonged stability by release impeding. Additionally, the particle size, distribution, and longevity of Ag-MOF NPs can affect the release rate of Ag^+[60−64] and therefore their antibacterial activity.[65] Similar to Ag NPs, Ag-MOF NPs are relatively unstable and their agglomeration significantly reduces their antibacterial activity.[64,66] The incorporation of GO nanosheets with numerous functional groups bearing oxygen results in smaller size, uniform distribution, and higher surface contact area of the GO−Ag-MOF compared with Ag-MOF, overcoming those aforementioned limitations to attain slower Ag^+ release rate and hence improving antibacterial activity.[48,67,68]

3.5. Transport Properties of Membranes. Results of the evaluation of the separation performance of each of the membranes (obtained from FO experiments using a salt solution as the drawing agent) are presented in Table 3. Water permeability (A) and solute permeability (B) coefficients were obtained using a four-step protocol described in literature.[69] Figure 13 and Table 3 indicate that the GO membrane has higher water and solute permeabilities due to its higher hydrophilicity than the TFC membrane, and it has a smoother surface than the other TFN membranes. Furthermore, higher porosity and specific surface area (discussed in previous work[14]) of the GO nanosheets provide more paths with more tortuosity for selective water transport, leading to a higher permselectivity indicated by the lower B/A ratio. Compared with the GO TFN membrane, the GO−Ag-MOF TFN membrane showed higher water permeability and selectivity. The higher negativity of the membrane surface results in a stronger Donnan effect, and consequently in a higher salt retention, leading to a lower B/A ratio. This surface charge also

DOI: 10.1021/acsami.8b12714
ACS Appl. Mater. Interfaces 2018, 10, 42967−42978

Table 3. Transport Properties of the Membranes

membrane	A^a	B^a	B/A (1/bar)	R_{JW}^{2a}	R_{JS}^{2a}
TFC	1.15 ± 0.13	0.15 ± 0.03	0.13 ± 0.08	0.97	0.98
GO TFN	2.75 ± 0.16	0.25 ± 0.03	0.08 ± 0.03	0.98	0.97
Ag-MOF TFN	1.70 ± 0.16	0.19 ± 0.02	0.11 ± 0.05	0.98	0.97
GO-Ag-MOF TFN	2.45 ± 0.14	0.21 ± 0.03	0.09 ± 0.04	0.96	0.99

[a] A: water permeability coefficient (L/(m^2·h·bar)). B: solute permeability coefficient (L/(m^2·h)). R_{JW}^2: water flux coefficient of determination. R_{JS}^2: solute flux coefficient of determination.

lowers the fouling rate, which agrees well with the antifouling results (Figure 12a).

4. CONCLUSIONS

This paper presented a novel TFN membrane that has enhanced biofouling and fouling resistances. The membrane was fabricated by embedding an Ag-based MOF decorated with GO into the membrane active layer. The high hydrophilic nature of the GO−Ag-MOF nanomaterials led to enhanced surface hydrophilicity of GO−Ag-MOF TFN membrane. FO experiments with feed-containing *E. coli* and sodium alginate pointed to outstanding anti-biofouling and antifouling properties of the GO−Ag-MOF TFN membrane. Furthermore, FI showed higher inhibition of bacteria deposition for the GO−Ag-MOF TFN membrane than the Ag-MOF and GO TFN, and the TFC membranes. In addition to enhanced hydrophilicity and biocidal activity, higher negative surface charge of the GO−Ag-MOF TFN membrane contributed to the exceptional anti-biofouling properties of the membrane.

■ ASSOCIATED CONTENT

Supporting Information

The Supporting Information is available free of charge on the ACS Publications website at DOI: 10.1021/acsami.8b12714.

Schematic interaction between GO and Ag-MOF crystals; schematic representation of the FO setup; EDX spectroscopy of the Ag-MOF and GO−Ag-MOF membranes; and elemental compositions of the fabricated membranes obtained from an EDX analysis of the top surface of each membrane (PDF)

■ AUTHOR INFORMATION

Corresponding Authors

*E-mail: ahmadrahimpour@nit.ac.ir (A.R.).
*E-mail: mesfahani@eng.ua.edu (M.R.E.).
*E-mail: soroushm@drexel.edu (M.S.).

ORCID

Mostafa Dadashi Firouzjaei: 0000-0002-0215-8210
Ahmad Arabi Shamsabadi: 0000-0002-9726-2466
Masoud Soroush: 0000-0002-4879-5098

Author Contributions

#M.D.F. and A.A.S. contributed equally to this work.

Notes

The authors declare no competing financial interest.

■ ACKNOWLEDGMENTS

A.A.S. was partially supported by the U.S. National Science Foundation under grant no. CBET-1804285. Any opinions, findings, and conclusions or recommendations expressed in this material are those of the authors and do not necessarily reflect the views of the National Science Foundation.

■ REFERENCES

(1) Pedro-Monzonís, M.; Solera, A.; Ferrer, J.; Estrela, T.; Paredes-Arquiola, J. A Review of Water Scarcity and Drought Indexes in Water Resources Planning and Management. *J. Hydrol.* **2015**, *527*, 482−493.

(2) Zhang, X.; Zhang, T.; Ng, J.; Sun, D. D. High-Performance Multifunctional TiO_2 Nanowire Ultrafiltration Membrane with a Hierarchical Layer Structure for Water Treatment. *Adv. Funct. Mater.* **2009**, *19*, 3731−3736.

(3) Mauter, M. S.; Zucker, I.; Perreault, F.; Werber, J. R.; Kim, J.-H.; Elimelech, M. The Role of Nanotechnology in Tackling Global Water Challenges. *Nat. Sustain.* **2018**, *1*, 166−175.

(4) Shannon, M. A.; Bohn, P. W.; Elimelech, M.; Georgiadis, J. G.; Mariñas, B. J.; Mayes, A. M. Science and Technology for Water Purification in the Coming Decades. *Nature* **2008**, *452*, 301−310.

(5) Rahimpour, A.; Seyedpour, S. F.; Aghapour Aktij, S.; Dadashi Firouzjaei, M.; Zirehpour, A.; Arabi Shamsabadi, A.; Khoshhal Salestan, S.; Jabbari, M.; Soroush, M. Simultaneous Improvement of Antimicrobial, Antifouling, and Transport Properties of Forward Osmosis Membranes with Immobilized Highly-Compatible Polyrhodanine Nanoparticles. *Environ. Sci. Technol.* **2018**, *52*, 5246−5258.

(6) Lutchmiah, K.; Verliefde, A. R. D.; Roest, K.; Rietveld, L. C.; Cornelissen, E. R. Forward Osmosis for Application in Wastewater Treatment: A Review. *Water Res.* **2014**, *58*, 179−197.

(7) Shaffer, D. L.; Werber, J. R.; Jaramillo, H.; Lin, S.; Elimelech, M. Forward Osmosis: Where Are We Now? *Desalination* **2015**, *356*, 271−284.

(8) Chen, W.; Su, Y.; Peng, J.; Dong, Y.; Zhao, X.; Jiang, Z. Engineering a Robust, Versatile Amphiphilic Membrane Surface Through Forced Surface Segregation for Ultralow Flux-Decline. *Adv. Funct. Mater.* **2011**, *21*, 191−198.

(9) Kang, G.-d.; Cao, Y.-m. Development of Antifouling Reverse Osmosis Membranes for Water Treatment: A Review. *Water Res.* **2012**, *46*, 584−600.

(10) Seyedpour, S. F.; Rahimpour, A.; Shamsabadi, A. A.; Soroush, M. Improved Performance and Antifouling Properties of Thin-Film Composite Polyamide Membranes Modified with Nano-Sized Bactericidal Graphene Quantum Dots for Forward Osmosis. *Chem. Eng. Res. Des.* **2018**, *139*, 321.

(11) Zhang, Q.; Jie, Y. W.; Loong, W. L. C.; Zhang, J.; Fane, A. G.; Kjelleberg, S.; Rice, S. A.; McDougald, D. Characterization of Biofouling in a Lab-Scale Forward Osmosis Membrane Bioreactor (FOMBR). *Water Res.* **2014**, *58*, 141−151.

(12) Coday, B. D.; Heil, D. M.; Xu, P.; Cath, T. Y. Effects of Transmembrane Hydraulic Pressure on Performance of Forward Osmosis Membranes. *Environ. Sci. Technol.* **2013**, *47*, 2386−2393.

(13) Linares, R. V.; Li, Z.; Sarp, S.; Bucs, S. S.; Amy, G.; Vrouwenvelder, J. S. Forward Osmosis Niches in Seawater Desalination and Wastewater Reuse. *Water Res.* **2014**, *66*, 122−139.

(14) Firouzjaei, M. D.; Shamsabadi, A. A.; Sharifian Gh., M.; Rahimpour, A.; Soroush, M. A Novel Nanocomposite with Superior Antibacterial Activity: A Silver-Based Metal Organic Framework Embellished with Graphene Oxide. *Adv. Mater. Interfaces* **2018**, *5*, 1701365.

(15) Wang, J.; Li, J.; Qian, S.; Guo, G.; Wang, Q.; Tang, J.; Shen, H.; Liu, X.; Zhang, X.; Chu, P. K. Antibacterial Surface Design of Titanium-Based Biomaterials for Enhanced Bacteria-Killing and Cell-Assisting Functions against Periprosthetic Joint Infection. *ACS Appl. Mater. Interfaces* **2016**, *8*, 11162−11178.

DOI: 10.1021/acsami.8b12714
ACS Appl. Mater. Interfaces 2018, 10, 42967−42978

(16) Kim, I. Y.; Park, S.; Kim, H.; Park, S.; Ruoff, R. S.; Hwang, S.-J. Strongly-Coupled Freestanding Hybrid Films of Graphene and Layered Titanate Nanosheets: An Effective Way to Tailor the Physicochemical and Antibacterial Properties of Graphene Film. *Adv. Funct. Mater.* **2014**, *24*, 2288−2294.
(17) Schwartz, V. B.; Thétiot, F.; Ritz, S.; Pütz, S.; Choritz, L.; Lappas, A.; Förch, R.; Landfester, K.; Jonas, U. Antibacterial Surface Coatings from Zinc Oxide Nanoparticles Embedded in Poly(N-isopropylacrylamide) Hydrogel Surface Layers. *Adv. Funct. Mater.* **2012**, *22*, 2376−2386.
(18) Zirehpour, A.; Rahimpour, A.; Khoshhal, S.; Firouzjaei, M. D.; Ghoreyshi, A. A. The Impact of MOF Feasibility to Improve the Desalination Performance and Antifouling Properties of FO Membranes. *RSC Adv.* **2016**, *6*, 70174−70185.
(19) Ben-Sasson, M.; Zodrow, K. R.; Genggeng, Q.; Kang, Y.; Giannelis, E. P.; Elimelech, M. Surface Functionalization of Thin-Film Composite Membranes with Copper Nanoparticles for Antimicrobial Surface Properties. *Environ. Sci. Technol.* **2013**, *48*, 384−393.
(20) Etacheri, V.; Michlits, G.; Seery, M. K.; Hinder, S. J.; Pillai, S. C. A Highly Efficient $TiO_{2-x}C_x$ Nano-heterojunction Photocatalyst for Visible Light Induced Antibacterial Applications. *ACS Appl. Mater. Interfaces* **2013**, *5*, 1663−1672.
(21) He, W.; Kim, H.-K.; Wamer, W. G.; Melka, D.; Callahan, J. H.; Yin, J.-J. Photogenerated Charge Carriers and Reactive Oxygen Species in ZnO/Au Hybrid Nanostructures with Enhanced Photocatalytic and Antibacterial Activity. *J. Am. Chem. Soc.* **2013**, *136*, 750−757.
(22) Chen, X.; Selloni, A. *Introduction: Titanium Dioxide (TiO_2) Nanomaterials*; ACS Publications, 2014.
(23) Franci, G.; Falanga, A.; Galdiero, S.; Palomba, L.; Rai, M.; Morelli, G.; Galdiero, M. Silver Nanoparticles as Potential Antibacterial Agents. *Molecules* **2015**, *20*, 8856−8874.
(24) Qiu, S.; Xue, M.; Zhu, G. Metal-organic framework membranes: from synthesis to separation application. *Chem. Soc. Rev.* **2014**, *43*, 6116−6140.
(25) Wyszogrodzka, G.; Marszałek, B.; Gil, B.; Dorożyński, P. Metal-Organic Frameworks: Mechanisms of Antibacterial Action and Potential Applications. *Drug Discovery Today* **2016**, *21*, 1009−1018.
(26) Horcajada, P.; Gref, R.; Baati, T.; Allan, P. K.; Maurin, G.; Couvreur, P.; Férey, G.; Morris, R. E.; Serre, C. Metal-Organic Frameworks in Biomedicine. *Chem. Rev.* **2011**, *112*, 1232−1268.
(27) Berchel, M.; Le Gall, T.; Denis, C.; Le Hir, S.; Quentel, F.; Elléouet, C.; Montier, T.; Rueff, J.-M.; Salaün, J.-Y.; Haelters, J.-P.; Hix, G. B.; Lehn, P.; Jaffrès, P.-A. A silver-based metal-organic framework material as a "reservoir" of bactericidal metal ions. *New J. Chem.* **2011**, *35*, 1000−1003.
(28) Lu, X.; Ye, J.; Zhang, D.; Xie, R.; Bogale, R. F.; Sun, Y.; Zhao, L.; Zhao, Q.; Ning, G. Silver carboxylate metal-organic frameworks with highly antibacterial activity and biocompatibility. *J. Inorg. Biochem.* **2014**, *138*, 114−121.
(29) He, C.; Liu, D.; Lin, W. Nanomedicine Applications of Hybrid Nanomaterials Built from Metal-Ligand Coordination Bonds: Nanoscale Metal-Organic Frameworks and Nanoscale Coordination Polymers. *Chem. Rev.* **2015**, *115*, 11079−11108.
(30) Wang, X.; Zhao, D.; Tian, A.; Ying, J. Three 3D silver-bis(triazole) metal-organic frameworks stabilized by high-connected Wells-Dawson polyoxometallates. *Dalton Trans.* **2014**, *43*, 5211−5220.
(31) Mangadlao, J. D.; Santos, C. M.; Felipe, M. J. L.; de Leon, A. C. C.; Rodrigues, D. F.; Advincula, R. C. On the Antibacterial Mechanism of Graphene Oxide (GO) Langmuir−Blodgett Films. *Chem. Commun.* **2015**, *51*, 2886−2889.
(32) Akhavan, O.; Ghaderi, E. Toxicity of Graphene and Graphene Oxide Nanowalls against Bacteria. *ACS Nano* **2010**, *4*, 5731−5736.
(33) Tang, J.; Chen, Q.; Xu, L.; Zhang, S.; Feng, L.; Cheng, L.; Xu, H.; Liu, Z.; Peng, R. Graphene Oxide-Silver Nanocomposite As a Highly Effective Antibacterial Agent with Species-Specific Mechanisms. *ACS Appl. Mater. Interfaces* **2013**, *5*, 3867−3874.
(34) Hu, M.; Mi, B. Enabling Graphene Oxide Nanosheets as Water Separation Membranes. *Environ. Sci. Technol.* **2013**, *47*, 3715−3723.
(35) Seabra, A. B.; Paula, A. J.; de Lima, R.; Alves, O. L.; Durán, N. Nanotoxicity of Graphene and Graphene Oxide. *Chem. Res. Toxicol.* **2014**, *27*, 159−168.
(36) Zirehpour, A.; Rahimpour, A.; Arabi Shamsabadi, A.; Sharifian Gh., M.; Soroush, M. Mitigation of Thin-Film Composite Membrane Biofouling via Immobilizing Nano-Sized Biocidal Reservoirs in the Membrane Active Layer. *Environ. Sci. Technol.* **2017**, *51*, 5511−5522.
(37) Kang, S. M.; Park, S.; Kim, D.; Park, S. Y.; Ruoff, R. S.; Lee, H. Simultaneous Reduction and Surface Functionalization of Graphene Oxide by Mussel-Inspired Chemistry. *Adv. Funct. Mater.* **2011**, *21*, 108−112.
(38) Zirehpour, A.; Rahimpour, A.; Arabi Shamsabadi, A.; Sharifian Gh., M.; Soroush, M. Mitigation of Thin-Film Composite Membrane Biofouling via Immobilizing Nano-Sized Biocidal Reservoirs in the Membrane Active Layer. *Environ. Sci. Technol.* **2017**, *51*, 5511−5522.
(39) Ghanbari, M.; Emadzadeh, D.; Lau, W. J.; Matsuura, T.; Ismail, A. F. Synthesis and Characterization of Novel Thin Film Nanocomposite Reverse Osmosis Membranes with Improved Organic Fouling Properties for Water Desalination. *RSC Adv.* **2015**, *5*, 21268−21276.
(40) Rahimpour, A.; Jahanshahi, M.; Mollahosseini, A.; Rajaeian, B. Structural and Performance Properties of UV-Assisted TiO_2 Deposited Nano-Composite PVDF/SPES Membranes. *Desalination* **2012**, *285*, 31−38.
(41) Wei, X.; Wang, Z.; Wang, J.; Wang, S. A Novel Method of Surface Modification to Polysulfone Ultrafiltration Membrane by Preadsorption of Citric Acid or Sodium Bisulfite. *Membr. Water Treat.* **2012**, *3*, 35−49.
(42) Baig, M. I.; Ingole, P. G.; Choi, W. K.; Jeon, J.-d.; Jang, B.; Moon, J. H.; Lee, H. K. Synthesis and Characterization of Thin Film Nanocomposite Membranes Incorporated with Surface Functionalized Silicon Nanoparticles for Improved Water Vapor Permeation Performance. *Chem. Eng. J.* **2017**, *308*, 27−39.
(43) Silverstein, R. M.; Webster, F. X.; Kiemle, D. J.; Bryce, D. L. *Spectrometric Identification of Organic Compounds*; John Wiley & Sons, 2014.
(44) Jahan, M.; Bao, Q.; Yang, J.-X.; Loh, K. P. Structure-Directing Role of Graphene in the Synthesis of Metal−Organic Framework Nanowire. *J. Am. Chem. Soc.* **2010**, *132*, 14487−14495.
(45) Jahan, M.; Liu, Z.; Loh, K. P. A Graphene Oxide and Copper-Centered Metal Organic Framework Composite as a Tri-Functional Catalyst for HER, OER, and ORR. *Adv. Funct. Mater.* **2013**, *23*, 5363−5372.
(46) Khorshidi, B.; Thundat, T.; Fleck, B. A.; Sadrzadeh, M. Thin Film Composite Polyamide Membranes: Parametric Study on the Influence of Synthesis Conditions. *RSC Adv.* **2015**, *5*, 54985−54997.
(47) Park, S.-H.; Kim, S. H.; Park, S.-J.; Ryoo, S.; Woo, K.; Lee, J. S.; Kim, T.-S.; Park, H.-D.; Park, H.; Park, Y.-I.; Cho, J.; Lee, J.-H. Direct Incorporation of Silver Nanoparticles onto Thin-Film Composite Membranes via Arc Plasma Deposition for Enhanced Antibacterial and Permeation Performance. *J. Membr. Sci.* **2016**, *513*, 226−235.
(48) Soroush, A.; Ma, W.; Silvino, Y.; Rahaman, M. S. Surface Modification of Thin Film Composite Forward Osmosis Membrane by Silver-Decorated Graphene-Oxide Nanosheets. *Environ. Sci.: Nano* **2015**, *2*, 395−405.
(49) Tang, C.; Kwon, Y.; Leckie, J. Probing the nano- and micro-scales of reverse osmosis membranes-A comprehensive characterization of physiochemical properties of uncoated and coated membranes by XPS, TEM, ATR-FTIR, and streaming potential measurements. *J. Membr. Sci.* **2007**, *287*, 146−156.
(50) Boussu, K.; De Baerdemaeker, J.; Dauwe, C.; Weber, M.; Lynn, K. G.; Depla, D.; Aldea, S.; Vankelecom, I. F. J.; Vandecasteele, C.; Van der Bruggen, B. Physico-Chemical Characterization of Nanofiltration Membranes. *ChemPhysChem* **2007**, *8*, 370−379.
(51) Benavente, J.; Vázquez, M. I. Effect of Age and Chemical Treatments on Characteristic Parameters for Active and Porous

DOI: 10.1021/acsami.8b12714
ACS Appl. Mater. Interfaces 2018, 10, 42967−42978

Sublayers of Polymeric Composite Membranes. *J. Colloid Interface Sci.* **2004**, *273*, 547−555.
(52) Briggs, D.; Beamson, G. XPS Studies of the Oxygen 1s and 2s Levels in a Wide Range of Functional Polymers. *Anal. Chem.* **1993**, *65*, 1517−1523.
(53) Jiang, J.-H.; Zhu, L.-P.; Zhang, H.-T.; Zhu, B.-K.; Xu, Y.-Y. Improved hydrodynamic permeability and antifouling properties of poly(vinylidene fluoride) membranes using polydopamine nanoparticles as additives. *J. Membr. Sci.* **2014**, *457*, 73−81.
(54) Xu, L.; Xu, J.; Shan, B.; Wang, X.; Gao, C. Novel Thin-Film Composite Membranes via Manipulating the Synergistic Interaction of Dopamine and m-Phenylenediamine for Highly Efficient Forward Osmosis Desalination. *J. Mater. Chem. A* **2017**, *5*, 7920−7932.
(55) Xiu, Z.-m.; Zhang, Q.-b.; Puppala, H. L.; Colvin, V. L.; Alvarez, P. J. J. Negligible Particle-Specific Antibacterial Activity of Silver Nanoparticles. *Nano Lett.* **2012**, *12*, 4271−4275.
(56) Ocsoy, I.; Paret, M. L.; Ocsoy, M. A.; Kunwar, S.; Chen, T.; You, M.; Tan, W. Nanotechnology in Plant Disease Management: DNA-Directed Silver Nanoparticles on Graphene Oxide as an Antibacterial against Xanthomonas Perforans. *ACS Nano* **2013**, *7*, 8972−8980.
(57) Ma, W.; Soroush, A.; Van Anh Luong, T.; Rahaman, M. S. Cysteamine- and graphene oxide-mediated copper nanoparticle decoration on reverse osmosis membrane for enhanced anti-microbial performance. *J. Colloid Interface Sci.* **2017**, *501*, 330−340.
(58) Goncalves, G.; Marques, P. A. A. P.; Granadeiro, C. M.; Nogueira, H. I. S.; Singh, M. K.; Grácio, J. Surface Modification of Graphene Nanosheets with Gold Nanoparticles: The Role of Oxygen Moieties at Graphene Surface on Gold Nucleation and Growth. *Chem. Mater.* **2009**, *21*, 4796−4802.
(59) Kim, Y.-K.; Han, S. W.; Min, D.-H. Graphene Oxide Sheath on Ag Nanoparticle/Graphene Hybrid Films as an Antioxidative Coating and Enhancer of Surface-Enhanced Raman Scattering. *ACS Appl. Mater. Interfaces* **2012**, *4*, 6545−6551.
(60) Zhao, R.; Lv, M.; Li, Y.; Sun, M.; Kong, W.; Wang, L.; Song, S.; Fan, C.; Jia, L.; Qiu, S.; Sun, Y.; Song, H.; Hao, R. Stable Nanocomposite Based on PEGylated and Silver Nanoparticles Loaded Graphene Oxide for Long-Term Antibacterial Activity. *ACS Appl. Mater. Interfaces* **2017**, *9*, 15328−15341.
(61) Choi, O.; Clevenger, T. E.; Deng, B.; Surampalli, R. Y.; Ross, L., Jr.; Hu, Z. Role of Sulfide and Ligand Strength in Controlling Nanosilver Toxicity. *Water Res.* **2009**, *43*, 1879−1886.
(62) Yang, X.; Gondikas, A. P.; Marinakos, S. M.; Auffan, M.; Liu, J.; Hsu-Kim, H.; Meyer, J. N. Mechanism of Silver Nanoparticle Toxicity Is Dependent on Dissolved Silver and Surface Coating in Caenorhabditis Elegans. *Environ. Sci. Technol.* **2011**, *46*, 1119−1127.
(63) Dal Lago, V.; França de Oliveira, L.; de Almeida Gonçalves, K.; Kobarg, J.; Borba Cardoso, M. Size-Selective Silver Nanoparticles: Future of Biomedical Devices with Enhanced Bactericidal Properties. *J. Mater. Chem.* **2011**, *21*, 12267−12273.
(64) Zhao, R.; Kong, W.; Sun, M.; Yang, Y.; Liu, W.; Lv, M.; Song, S.; Wang, L.; Song, H.; Hao, R. Highly Stable Graphene-Based Nanocomposite (GO−PEI−Ag) with Broad-Spectrum, Long-Term Antimicrobial Activity and Antibiofilm Effects. *ACS Appl. Mater. Interfaces* **2018**, *10*, 17617.
(65) Xie, X.; Mao, C.; Liu, X.; Zhang, Y.; Cui, Z.; Yang, X.; Yeung, K. W. K.; Pan, H.; Chu, P. K.; Wu, S. Synergistic Bacteria Killing through Photodynamic and Physical Actions of Graphene Oxide/Ag/Collagen Coating. *ACS Appl. Mater. Interfaces* **2017**, *9*, 26417−26428.
(66) Wang, H.; Zhou, Y.; Jiang, X.; Sun, B.; Zhu, Y.; Wang, H.; Su, Y.; He, Y. Simultaneous Capture, Detection, and Inactivation of Bacteria as Enabled by a Surface-Enhanced Raman Scattering Multifunctional Chip. *Angew. Chem., Int. Ed.* **2015**, *54*, 5132−5136.
(67) Ruiz, O. N.; Fernando, K. A. S.; Wang, B.; Brown, N. A.; Luo, P. G.; McNamara, N. D.; Vangsness, M.; Sun, Y.-P.; Bunker, C. E. Graphene Oxide: A Nonspecific Enhancer of Cellular Growth. *ACS Nano* **2011**, *5*, 8100−8107.
(68) Perdikaki, A.; Galeou, A.; Pilatos, G.; Prombona, A.; Karanikolos, G. N. Ion-Based Metal/Graphene Antibacterial Agents Comprising Mono-Ionic and Bi-Ionic Silver and Copper Species. *Langmuir* **2018**, *34*, 11156−11166.
(69) Tiraferri, A.; Yip, N. Y.; Straub, A. P.; Romero-Vargas Castrillon, S.; Elimelech, M. A Method for the Simultaneous Determination of Transport and Structural Parameters of Forward Osmosis Membranes. *J. Membr. Sci.* **2013**, *444*, 523−538.

DOI: 10.1021/acsami.8b12714
ACS Appl. Mater. Interfaces 2018, 10, 42967−42978